Performance evaluation of rigid inclusions for settlement control of grain silos in tropical soils

Juan Félix Rodríguez Rebolledo[1] (ID), Isabelle Moreira Santiago[1] (ID),

Heitor Cardoso Bernardes[1#] (ID), Thiago Augusto Mendes[2] (ID)

Article

Keywords
Grain silos
Rigid inclusions
Serviceability limit-state
3D numerical modeling
Finite element method
Tropical soils

Abstract

This study presents the evaluation of the performance of grain silos reinforced by rigid inclusions in soils of the Central-West region of Brazil, during its construction and operation. Therefore, a group of eight silos with 32.4 m in diameter, 30 m in height, and 12,000 t of storage capacity (each silo) was numerically analyzed using the three-dimensional Finite Element Method (FEM, Plaxis 3D). The stratigraphy of the Experimental Field of the University of Brasilia, Brazil (CEGUnB) was considered in the analysis. The performance of using a system of rigid inclusions to reinforce the soil beneath the raft was compared with the behavior of an isolated raft. Two models were developed: in the first one, an independent silo was considered, its behavior was analyzed during its construction and operation stages by varying the length of the inclusions; in the second model, the group of eight silos was considered and their behavior was studied for different combinations of loading. The rigid inclusions system proved to be an efficient foundation solution that allows controlling total and differential displacements during the construction and serviceability stages of the silo, helping to prevent the formation of cracks in the structural elements and grain contamination by the excessive opening of the raft-perimeter beam structural joint.

1. Introduction

Agriculture is one of Brazil's main economic drivers, and thus it is subject to constant infrastructure investments in the production, storage and distribution of grains throughout the country. In recent decades, the storage of grains has received special attention, with the increase in the construction of silos along the Central-West region of the country, which is responsible of around 50% of Brazil's total grain production (CONAB, 2022).

However, the combination of inadequate foundation design and difficult soil conditions is one of the main causes of pathologies in grain silos (Dogangun et al., 2009). Cylindrical metallic silos are common in Brazil. In this type of silo, the metallic superstructure is supported by a perimeter ring beam and a raft foundation placed directly on the ground (disconnected from the beam). Commonly, end-bearing piles are added to the ring beam and the central tunnel (used for the silo emptying), which leaves the soil beneath the raft without any type of reinforcement.

Large areas of the Brazilian Central-West region are covered by a detritus-laterite soil mantle from the Tertiary-Quaternary age called "porous clay". This superficial clay layer presents a porous and highly unstable structure, with high void ratio and low shear strength. Therefore, the most common pathologies observed in these conditions are related to the Serviceability Limit State (SLS), i.e., the development of total and differential settlements of the raft foundation and the opening of the structural joint between the raft and the perimeter beam. These displacements cause cracks in the structural elements, the contamination and wetting of the stored grain, and malfunction of the conveyor belts installed in the central tunnel, which are used for emptying the silo (Conciani, 2016), as shown by Bernardes et al. (2021) and in Figure 1.

Therefore, techniques to improve the foundation system are needed to ensure the proper functioning of the silos (Souza Filho, 2018). In this paper, the use of rigid inclusions technique is proposed and evaluated as a solution to control the total and differential settlements in silo foundations.

In addition to its common use as a foundation solution for road and railway embankments, due to its good performance (Briançon et al., 2015) and low cost compared to other solutions (Rodríguez-Rebolledo & Auvinet, 2006), rigid inclusions have been used more frequently as a deep foundation system for different types of structures, such as buildings (Combarieu,

Figure 1. (a) Crack in the raft foundation; (b) structural joint opening between the raft and the beam ring; (c) sealing of the joint after opening.

1990; Santoyo & Ovando, 2006; Rodríguez-Rebolledo & Auvinet, 2006; Briançon et al., 2015), bridges (Pecker, 2004), and storage tanks (Bernuy et al., 2018).

This article presents the evaluation of the performance of grain silos reinforced by rigid inclusions in soils characteristic of the Central-West region of Brazil, during its construction and operational stages, using three-dimensional numerical modeling. A silo of 32.4 m in diameter, 30 m in height, and 12,000 t of storage capacity was analyzed. The stratigraphy of the Experimental Field of the University of Brasilia, Brazil (CEGUnB) was considered.

Two alternatives of foundations to the silo base slab, which receives the grain load, were analyzed and compared: an isolated raft, and a raft over a soil reinforced by a system of rigid inclusions. In both alternatives, the foundation of the perimeter ring beam and the central tunnel were kept the same, composed by conventional pile groups.

Two models were developed: in the first one, an independent silo was considered, its behavior was analyzed during its filling and emptying, by varying the length of the inclusions. In the second model, a group of eight silos was considered and their behavior was studied for different combinations of filling and emptying.

2. Model geometry and dimensions

The case selected for this investigation comprises a group of eight grain silos built in 2014, in São Félix do Araguaia, in the state of Mato Grosso, Brazil (Site 1 in Figure 2). According to Bernardes et al. (2021), after the first cycle of loading and unloading of the silos (only two silos were used in this period), several cracks and excessive settlement were observed at the silo's raft foundation.
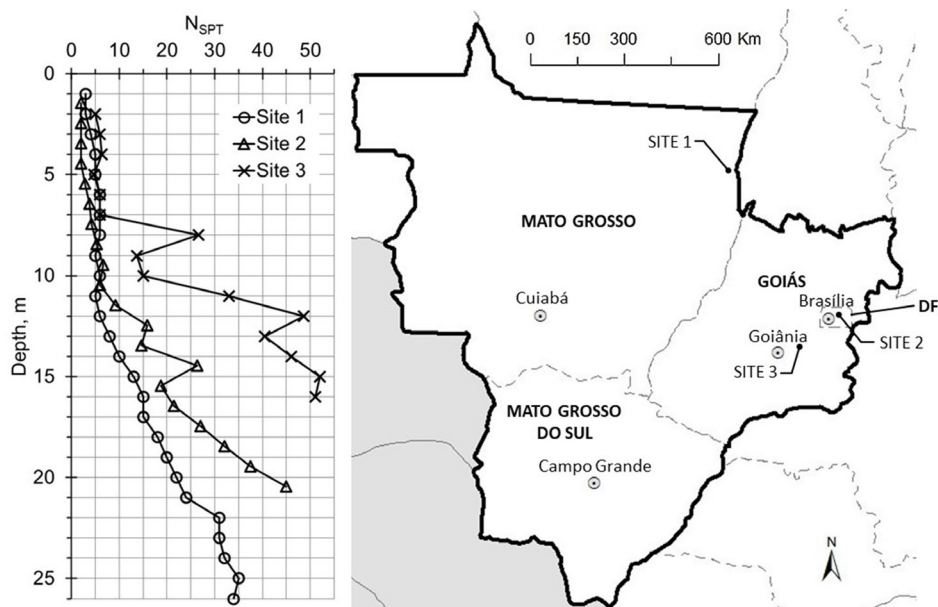
Figure 2. Standard penetration test results for different sites of silos projects within the Central-West region.

The wall and roof of each silo are made of a steel structure directly connected to a perimeter beam. Most of the grain weight is supported directly by a central raft, structurally disconnected from the perimeter beam and resting on an embankment of approximately 1.2 m thick (Figure 3). The raft is connected to a central tunnel and to eight aeration ducts, which provide a significant increase in the raft flexural stiffness. The foundation consists of continuous flight auger piles with 0.35 m in diameter and 20 m in length, disposed under the perimeter beam and the central tunnel, as shown previously in Bernardes et al. (2021).

The soil profile of the CEGUnB (Site 2 in Figure 2) was utilized in the analysis due to the stratigraphic conditions similar to the cases of silos with pathologies found in the Brazilian Central-West region (Sites 1 and 3 in Figure 2). Also, the large number of field and laboratory tests for the physical and mechanical characterization of the different soils of the CEGUnB contributed to a proper calibration of the soil constitutive model used in the numerical analysis considered herein (Perez, 1997; Jardim, 1998; Sales, 2000; Guimarães, 2002; Mota, 2003; Coelho, 2013; Sales et al., 2015).

Based on this information and the stratigraphic profiles proposed by Cruz (1987) and Cardoso (2002), Rodríguez-Rebolledo et al. (2019a) defined the soil profile of the CEGUnB. Superficially, an 8.5 m thick layer of detritus-lateritic soil composed mainly of red-yellow latosols. High degrees of weathering and leaching were responsible for the formation of this soil, which led to the development of a very porous, metastable aggregate structure with a large void ratio and, consequently, low density, called "porous clay" by local geotechnicians. Due to its high porosity and cementitious bond type, it has a highly unstable structure when subjected to increased moisture and/or changes in the
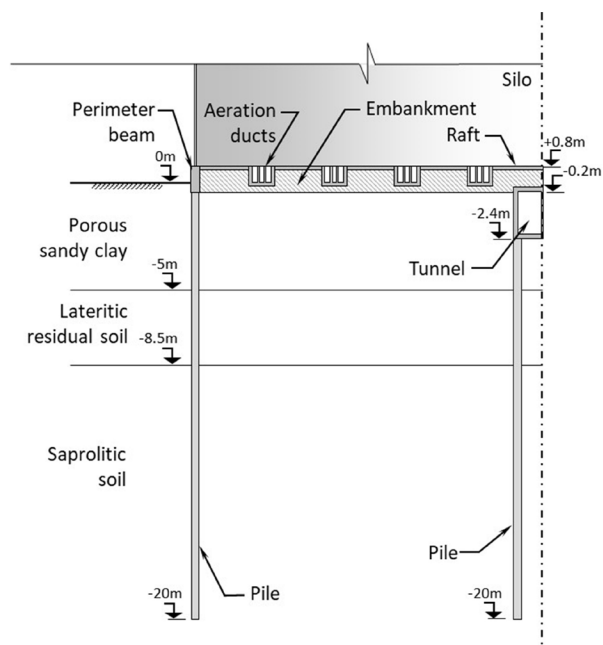
Figure 3. Original design of the silo's foundation.

stress state, which often lead to soil collapse. The end of the porous clay layer is identified in percussion drillings by the increase of N_{SPT} values from 8.5 to 10 m depth (transition layer), followed by the underlying saprolite soil.

3. Serviceability limit states

The Brazilian standard for foundations (ABNT, 2019) establishes that the serviceability limit value for a given

deformation is the one corresponding to any condition that compromises the proper performance of the structure, e.g., unacceptable cracks. The standard does not establish limit values, but it does establish the criteria that must be considered for its definition. There is not much experience in the technical and scientific literature related to the behavior of grain silos that would help us to define a value for the SLS, however, as is shown in the following, it is possible to find information on similar structures, such as the case of storage tanks, built on other difficult soils conditions, such as loose sands or soft clays.

The standard for steel tanks for oil storage (ABNT, 1983), mentions that foundations must be designed to avoid differential settlements that can cause distortions in the tank structure. Also, the design must minimize the total settlement, so that the bottom of the tank remains above the ground after its loading, and the pipelines connected to the tank are not subjected to high additional forces caused by the tank settlement.

Becker & Lo (1979) present the results of a research program on the foundation behavior of five tower silos on clay deposits in Southwestern Ontario, Canada. After the first loading cycle, one of the instrumented silos developed a maximum settlement at the ring foundation of about 78 mm, and at the center of the silo equal to 89 mm. From the performance survey of four other silos, the maximum settlement of the ring foundation varies from 30 to 109 mm. The authors conclude that the silos presented satisfactory performance concerning total and differential settlement, and tilting.

Based upon 31 case histories of tanks settlement and damage, D'Orazio & Duncan (1987) concluded that the allowable angular distortion (the slope between two adjacent points or columns) of steel tanks on compressible soils depends mainly on the shape of the settlement profile, which is critical in cases were the maximum settlement occur off-center.

Bernuy et al. (2018) consider a maximum allowable angular distortion of 1/300 for the foundation design of large diameter (96 m) liquefied natural gas tanks, which foundation was reinforced by rigid inclusions. The authors assessed the tank settlements under various load cases, which were equal to 50 mm for the empty case, 150 mm for the full tank, and 110 mm after the tank unloading.

The Indian standard (IS, 1986) for the design and construction of foundations, indicates allowable values of maximum and differential settlements for silos with shallow foundations, on sand, hard clay, or plastic clay. For raft foundations on sand or hard clay layer, 100 mm maximum settlement and 1/400 angular distortion are allowed, and on plastic clay layer, the limit values are 125 mm of maximum settlement and 1/400 of angular distortion.

Bahar et al. (2013) present the settlement observations of a cylindrical steel tank and ten steel silos founded on a reconstituted and compacted granular fill, in Algeria.

The authors concluded that the problems related to cracks and tilting in the monitored structures started from an angular distortion equal to 1/400.

Santrač et al. (2015) show the results of the measured and calculated settlements for a 17.7 m high silo, founded on a reinforced concrete slab, and subjected to a contact pressure of 190 kPa. The silo was constructed in Serbia, in a highly porous unsaturated layer of loess, which may exhibit collapse due to saturation. The total predicted settlement (initial compression, consolidation, and partial collapse) was equal to 183 mm, which is greater than the limit value established by the Serbia Technical Code (equal to 100 mm for the specified case). However, the settlements were uniform, not presenting potential damage to the silo's structure.

The literature review presented suggests that the maximum vertical settlement in silos and tanks remains between 89 and 183 mm, and the maximum angular distortion between 1/400 and 1/300. Therefore, this paper adopted the serviceability limit values of 150 mm and 1/400, for vertical settlement and angular distortion, respectively.

4. Numerical modeling description

Numerical modeling was developed using the Plaxis 3D software. The analysis was divided in two main parts: the individual behavior of a silo when changing the inclusions length, and the behavior of a group of eight silos considering different load combinations.

The rigid inclusions performance was evaluated by comparing the behavior of the silo's original foundation (piles only in the perimeter beam and in the tunnel, as described in Section 2) with one alternative solution, in which rigid inclusions were added under the silo's raft. As the objective of this research is to evaluate only the serviceability limit states, and the ultimate bearing capacity of the system was guaranteed by elements of the original foundation (Bernardes et al., 2021), this paper will not discuss the effect of the rigid inclusions on the foundation overall safety factor.

4.1 Stratigraphy and soil properties

Rodríguez-Rebolledo et al. (2019a) developed a methodology to obtain, adjust and validate the mechanical parameters of a typical soil profile (see the stratigraphy exposed in Figure 3) of the city of Brasília for the HS model (Hardening Soil Model), using laboratory and field test results obtained in previous studies conducted in the CEGUnB. The methodology presented began with the evaluation of the strength and compressibility parameters of triaxial CU tests (with isotropic and anisotropic consolidation) and one-dimensional consolidation tests, respectively (Guimarães, 2002). Then, the parameters obtained for the HS model were calibrated using the finite element method (FEM) and the SoilTest module of the Plaxis software. Based on the evaluation and calibration of these parameters, and the proposed soil

profile, a geotechnical model for natural moisture conditions (Nat.) was proposed, as shown in Table 1.

This geotechnical model was validated through numerical modeling of the load testing of footings and piles conducted in the CEGUnB (Sales, 2000; Guimarães, 2002). Using the same methodology and with the triaxial and consolidation tests performed by Guimarães (2002), Pérez-León (2017) determined the HS model parameters for the first 3.5 m of the porous clay layer in saturated state (Sat.), as shown in Table 1.

4.2 Properties for the distribution layer

For the distribution layer (improved soil), the Mohr-Coulomb model was adopted. Research performed by Otálvaro (2013) provided the estimates of the parameters for tropical soil improved by compaction that was used in this study (Table 2). The compacted tropical soil, of the laterite type and highly weathered, was collected from the city of Brasília. The material was classified as ML (low plasticity silt) according to the Unified Soil Classification System (USCS). The γ value was obtained from the results of Proctor Standard testing. Parameters E, ϕ›, and c’ were obtained from CD (consolidated-drained) triaxial tests performed on the same compacted soil. Echevarría (2006) obtained similar parameters for numerical simulations of tropical porous compacted soil.

4.3 Properties for the structural elements

For the modeling of the structural elements, all in concrete, the linear elastic constitutive model was assumed. Raft, perimeter beam, tunnel, and inclusions caps were modeled by plate elements; aeration ducts by beam elements; and piles and inclusions by embedded beams. Table 3 presents the parameters of the constitutive model adopted for each concrete element. The concrete Young's modulus was calculated according to the equation proposed in the Brazilian standard NBR 6118 (ABNT, 2014) as a function of the strength characteristics of the concrete subjected to simple compression. Therefore, a compressive stiffness of 25 GPa was assumed for the raft, perimeter beam, tunnel, piles, and inclusions caps, and 17.7 GPa for the inclusions. The Poisson's ratio of the concrete was equal to 0.2 for all elements (ABNT, 2014; ASIRI National Project, 2011).

The ultimate load capacity of the piles and rigid inclusions was evaluated using 2D axisymmetric FEM simulations (Plaxis 2D). The stratigraphic profile of CEGUnB and the geotechnical model for the HS were considered (Table 1). Concrete elements of 5, 10, 15, and 20 m in length and 0.35 m in diameter were modeled. Concrete-soil interface elements were inserted in the shaft and the tip of the pile, applying load increments on the pile head until the soil failure. For each simulation, a graph of applied load *versus* settlement was generated, where the load at failure for the point of maximum

Table 1. Geotechnical model proposed by the CEGUnB for the HS model (modified from Rodríguez-Rebolledo et al., 2019a).

Parameters	Layer number							
	1		2		3	4	5	6
	Porous sandy clay					Lateritic residual soil		Saprolitic soil
Depth (m)	0 - 1.5		1.5 - 3.5		3.5 - 5.0	5.0 - 7.0	7.0 - 8.5	8.5 - 20.0
State	Nat.	Sat.	Nat.	Sat.	Nat.	Nat.	Nat.	Nat.
γ (kN/m³)	13.1	16.5	12.8	16.4	13.9	14.3	16.0	18.2
c’ (kPa)	5	0	5	0	5	20	75	20
ϕ’ (°)	25	26	25	26	26	32	20	22
ψ (°)	0	0	0	0	0	0	0	0
E_{50}^{ref} (MPa)	3.2	2.2	2.5	2.1	4.0	12.0	13.2	12.2
E_{oed}^{ref} (MPa)	4.9	1.0	1.5	0.8	2.2	6.9	7.0	5.7
E_{ur}^{ref} (MPa)	14.0	13.0	14.0	13.0	36.9	37.5	54.0	54.0
m	0.50	0.65	0.50	0.80	0.50	0.50	0.50	0.70
v_{ur}	0.2	0.2	0.2	0.2	0.2	0.2	0.2	0.2
p^{ref} (kPa)	100	50	100	50	100	100	100	100
R_f	0.80	0.75	0.80	0.75	0.90	0.90	0.90	0.80
POP (kPa)	65.7	16.1	31.8	6.6	0.0	31.4	0.0	0.0
K_o^{nc}	0.58	0.56	0.58	0.56	0.56	0.47	0.66	0.63
K_o	1.37	0.75	0.77	0.75	0.56	0.56	0.66	0.63

γ: unit weight of moist soil, c’ and ϕ›: the effective shear strength parameters, ψ: dilatancy angle, E_{50}^{ref}: the reference secant stiffness modulus for the drained triaxial test, E_{oed}^{ref}: the reference tangent stiffness modulus for oedometric loading, E_{ur}^{ref}: the reference stiffness modulus for unloading and reloading conditions, m: the exponent that defines the strain dependence of the stress state, v_{ur}: unloading/reloading Poisson's ratio, p^{REF}: the reference isotropic stress, R_f: the failure ratio, POP: the pre-overburden pressure, K_o^{nc}: the coefficient of the earth pressure at rest for normal consolidation, and K_o: coefficient of earth pressure at rest.

curvature was calculated. Then, an axial load *versus* depth graph (for load at pile failure) was obtained, which allowed to define the tip and shaft resistances (Table 3).

Equations 1 and 2 (García-Buriticá et al., 2021) were used to determine the spacing between inclusions (*S*) and the diameter of the inclusion cap (*a*), considering the shear strength values indicated in Table 2 (*c'* = 80 kPa, ϕ = 38°), a distribution layer thickness (*H*) of 1.2 m and a uniformly distributed load applied on the raft (q_s) of 135.3 kPa. The ultimate load-bearing capacity of the inclusion cap (q_{ult}) was calculated using Equation 3 (García-Buriticá, 2021).

$$\frac{S_{min} - a}{a} = \sqrt{\frac{q_{ult}}{q_1}} - 1, \text{for } S = D \tag{1}$$

Table 2. Parameters for the distribution layer.

Parameter	Value
Unit weight, γ (kN/m³)	18.6
Young's modulus, E (MPa)	60
Cohesion, c' (kPa)	80
Friction angle, ϕ (°)	38
Poisson's ratio, ν	0.33

where S_{min} is the minimum value of S (obtained for $S = D$), D is the diameter of the top surface of the load transfer cone (LTC), and q_1 is the total pressure transmitted to the inclusion cap in terms of q_s and the shape of the LTC.

$$H_{max} = (S_{min} - a)\frac{\tan \beta}{2} \tag{2}$$

where H_{max} is the maximum value of H, and β is the external angle of the LTC defined by Colomb's theory as $45° + \phi'/2$.

$$q_{ult} = c'N_c s_c g_c \tag{3}$$

where s_c is the shape factor = $1 + N_q/N_c$, g_c is the inclination factor of the LTC ≈ 0.13 for $\phi' = 38°$ (according to García-Buriticá, 2021), and N_q and N_c are the bearing capacity factors. According to the above, were obtained values of $S = 2$ m and $a = 0.7$ m, which avoid the penetration of the inclusion cap in the distribution layer by punching and the transfer of point loads in the raft.

Table 3. Parameters for the structural elements.

a) Parameters for plate elements				
Parameter	Inclusion cap	Perimeter beam	Raft	Tunnel
Thickness, d (m)	0.1	0.4	0.2	0.2
Unit weight, γ (kN/m³)	24	24	24	24
Young's modulus, E (GPa)	25	25	25	25
Poisson's ratio, ν	0.2	0.2	0.2	0.2

b) Parameters for aeration ducts (beam elements)		
Parameter	Value	Cross section
Young's modulus, E (GPa)	25	
Unit weight, γ (kN/m³)	24	
Cross section, A (m²)	0.56	
Inertia around 2nd axis (m⁴)	0.0875	
Inertia around 3rd axis (m⁴)	0.0454	

c) Parameters for embedded beams					
Parameter	Piles		Inclusions		
Length, L_{pile} (m)	20	5	10	15	20
Young's modulus, E (GPa)	25.0	17.7	17.7	17.7	17.7
Unit weight, γ (kN/m³)	24	23	23	23	23
Diameter, D (m)	0.35	0.35	0.35	0.35	0.35
Side friction resistance, T_{sf} (kN/m)	53.6	18.7	42.6	53.6	66.3
Base resistance, F_{max} (kN)	37.2	46.9	30.6	37.2	46.3
Total resistance, N_{pile} (kN)*	841.2	140.4	456.6	841.2	1372.3

*$N_{pile} = F_{max} + L_{pile}T_{sf}$
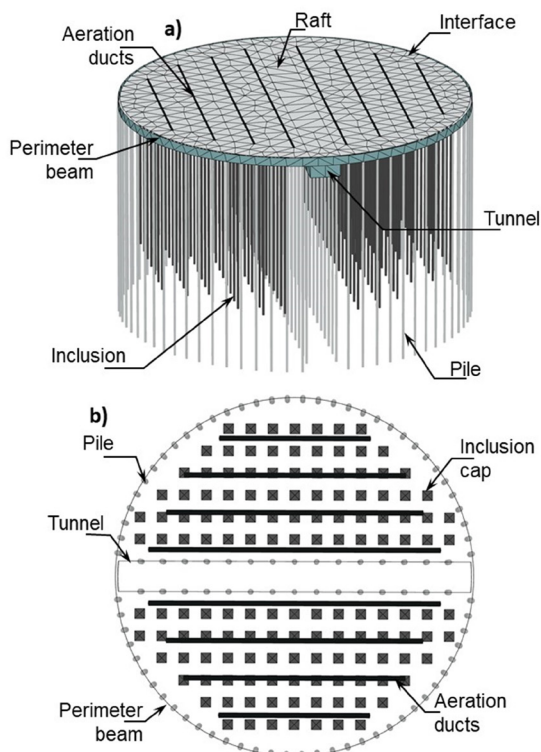
4.4 Cases analyzed and stages

The finite element mesh developed for the silo's foundation is presented in Figure 4. For the simulation of the perimeter joint, a space of 200 mm was left between the raft and the perimeter beam, and an interface element was placed between the embankment (load transfer platform) and the perimeter beam.

For the case of the individual silo, after a sensitivity analysis, the lateral boundaries of the finite element mesh were placed at a distance of approximately three times the diameter of the silo (100 m from the silo axis in the x and y directions). The lower boundary was established at a depth of 25 m, beyond which the N_{SPT} was larger than 40 blows, and the soil was classified as very compact, according to the Brazilian standard NBR 6484 (ABNT, 2001).

Only a quarter of the silo's plan geometry could have been simulated, as adopted by Móczár et al. (2016) in a sugar silo analysis, but it was decided to model the complete silo because it served as a calibration for its use in the group modeling, i.e., for the generation of the model that considers a group of silos.

The medium was discretized by a finite element mesh with 71,409 10-node tetrahedral elements, which proved to be enough according to sensitivity analyses. The lateral boundary conditions were fixed in the horizontal direction, and the bottom boundary conditions were fixed in both directions.

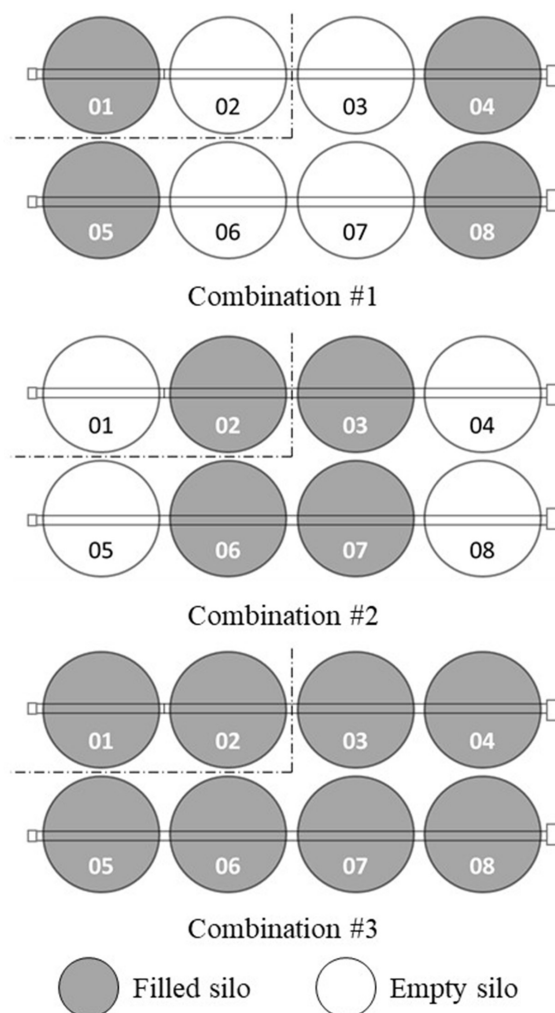As shown in Figure 5, for modeling of the interaction between the group of eight silos during the filling and emptying processes, the symmetry conditions of the problem were considered and three possible combinations were defined. The lateral boundaries of the finite element mesh were placed at a distance approximately three times the diameter of the silo (100 m from Silo 01 axis in the x direction and 100 m from Silos 01 and 02 in the y direction). The boundary conditions were set as the same used for the isolated silo model.

Table 4 shows the stages of analysis used for all the studied cases. The loads on the raft and the perimeter beam were obtained from the original project and correspond to the service loads for the silo working at its maximum capacity.

5. Analysis of the results

5.1 Case 1: individual behavior

The maximum vertical displacements (ρ^{MAX}) obtained at the silo raft, for the cases with the original foundation

Figure 4. General configuration of the finite element mesh developed for the silo's foundations: (a) 3D; (b) plan view.

Figure 5. Possible combinations for the analysis of the interaction between the eight silos.

Table 4. Stages of analysis.

Stage	Characteristics
1	Initial stress conditions
2	Silo construction. Applied load on the perimeter beam = 183.1 kN/m
3	Total filling of the silo. Applied load on the silo raft = 135.3 kPa
4	Total discharge of the silo raft.

Figure 6. Maximum vertical displacement obtained at the silo raft, for the original foundation solution considering: (a) natural; (b) saturated conditions; (c) reinforced with rigid inclusions considering both moistures states.

solution and reinforced with rigid inclusions, for stages 3 and 4 (total filling and discharge of the silo, respectively), and for stratigraphic conditions of natural and saturated moisture states, are shown in Figure 6.

It is possible to observe that for the original foundation solution, considering the natural condition (Figure 6a), ρ^{MAX} = 34 cm when the silo is completely filled, and when it is completely emptied a ρ^{MAX} = 24 cm remains. This means that after the loading of the silo a permanent (plastic) displacement is developed, equivalent to 70% of the total, and an elastic value remains of approximately 10 cm that may develop during the loading-unloading cycles of the silo.

In a saturated condition (Figure 6b) the settlement increases to ρ^{MAX} = 46 cm when the silo is loaded, and ρ^{MAX} = 37 cm after unloading, which corresponds to an increase of 35% in the total settlements and 54% in the permanent ones. It is possible to say that all these displacement values considerably exceed the adopted limit-state for total vertical displacements (15 cm).

When rigid inclusions of 15 m length are added, the ρ^{MAX} values are reduced by 78%, i.e., to 10 cm and 8 cm (Figure 6c), for total and permanent, respectively, and therefore the remaining elastic displacement is only 2 cm.

Figure 7 shows the vertical displacements obtained at the silo raft, at the perimeter beam, and the tunnel, for the cases with the original foundation solution and reinforced with rigid inclusions, for stage 3 (total filling), and for the natural condition.

For the original foundation (Figures 7a) occurs the development of displacements with considerably different magnitudes within each structural element and between them. For the raft, as mentioned before, when the silo is loaded, the maximum displacement is equal to 340 mm (located in the center of the black zone); and the minimum displacement (ρ^{MIN}) is about 120 mm, located at the ends of the tunnel (in the greyish zone), at a distance (L) of about 7.5 m. These results generate an angular distortion in the silo raft ($\delta_{max} = \left(\rho^{max} - \rho^{min} \right) / L$) equal to 1/34, well above the adopted limit-state (1/400). For the tunnel structure, despite being reinforced with piles, total displacements of ρ^{MAX} = 17 cm and δ^{MAX} = 1/326 were obtained, both values above the limit state. For the case of the perimeter beam, due to the reinforcement with piles and the low magnitude of transmitted load (compared to the tunnel) a total displacement of 10 cm and angular distortion of 1/796 were obtained.
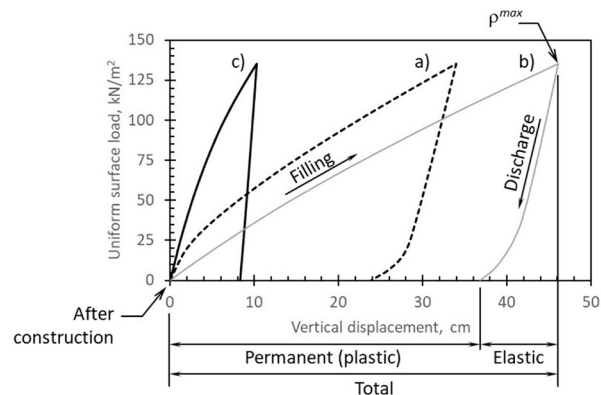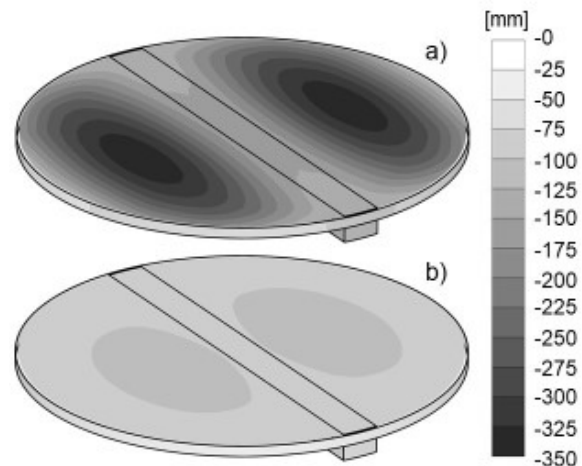

Figure 7. Vertical displacements computed for stage 3 at the silo raft, perimeter beam, and tunnel, considering a natural moisture state: (a) for the original foundation solution; (b) when reinforced with rigid inclusions.

When the rigid inclusions are added (Figure 7b) there is a significant reduction in differential displacements on the raft, i.e., ρ^{MAX} reduces to 10 cm, ρ^{MIN} to 8 cm, and L increases to 10.2 m, leading to an angular distortion of only 1/510, and for the tunnel, ρ^{MAX} reduces to 9.5 cm and δ^{MAX} to 1/1000 (i.e., both structures below the established limits).

Another important differential displacement that is observed in the silo (Figure 8), is the one that develops between the perimeter beam and the raft. Since the perimeter beam is strongly reinforced by piles, the vertical displacement is considerably lower than that developed in the perimeter of the raft, generating a gap between both elements when the silo is filled. This gap may cause grain contamination and structure service failure (Figure 1b).
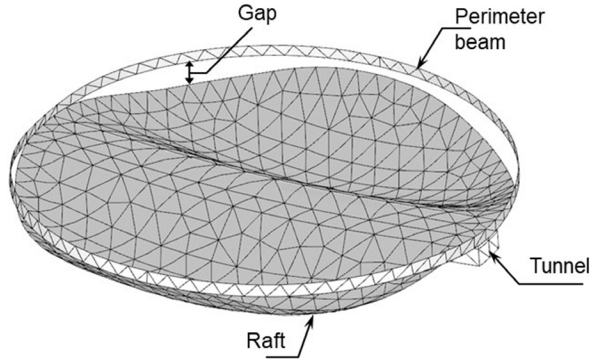
Figure 8. Deformed mesh obtained when the silo is filled (scaled up 20 times).

According to the obtained results, the maximum gap value obtained (G^{MAX}) is about 15.2 cm (stage 3, total displacement), and 11.5 cm when empty (stage 4, permanent displacement). For the foundation reinforced by rigid inclusions, $G^{MAX} = 2.4$ cm for stage 3 and $G^{MAX} = 1.4$ cm for stage 4, hence, a remaining elastic displacement of only 1 cm. It means that the inclusions allow the raft and beam to settle more uniformly, allowing the value of the gap to be reduced by approximately 85%.

For a better understanding of the foundation's performance when the rigid inclusions are added, a parametric analysis was performed by varying the length of these elements. Then, the results of the maximum displacement predictions were compared with those obtained when using the original foundation solution. According to Rodríguez-Rebolledo et al. (2019b), three relationships can be proposed that allowed evaluating the performance of the foundation with rigid inclusions, these are: settlement reduction factor (*SRF*, Equation 4), angular distortion reduction factor (*DRF*, Equation 5) and raft-perimeter beam gap opening reduction factor (*GRF*, Equation 6).

$$SRF = 1 - \frac{\rho_{w/i}^{max}}{\rho_{w/o}^{max}} \tag{4}$$

where $\rho_{w/i}^{max}$ is the maximum vertical displacement obtained when rigid inclusions are included and $\rho_{w/o}^{max}$ is the maximum vertical displacement obtained for the original foundation solution. When *SRF* = 1, the settlement is fully reduced, and the performance of the inclusion system is at the maximum; when *SRF* = 0, the settlement reduction is null, and the performance of the system is at the minimum.

$$DRF = 1 - \frac{\delta_{w/i}^{max}}{\delta_{w/o}^{max}} \tag{5}$$

where $\delta_{w/i}^{max}$ is the maximum angular distortion obtained when rigid inclusions are added and $\delta_{w/o}^{max}$ is the maximum angular distortion obtained for the original foundation solution.

$$GRF = 1 - \frac{G_{w/i}^{max}}{G_{w/o}^{max}} \tag{6}$$

where $G_{w/i}^{max}$ is the maximum gap opening obtained with the use of rigid inclusions and $G_{w/o}^{max}$ is the maximum gap opening obtained for the original foundation.

The graphs in Figure 9 show the total and permanent values obtained for *SRF* and *DRF*, for the raft, the tunnel, and the perimeter beam, for inclusions lengths from 5 to 20 m. For the case of the raft, it is possible to observe that, from 10 m in length, a good performance of the proposed foundation system is obtained. The value of *SRF* ranges from 0.50 to 0.81 and from 0.38 to 0.79 for total and permanent displacements, respectively. This means that the inclusions were able to reduce the maximum vertical displacement by up to 80%, and to meet the serviceability limits for total displacements value (T-SLS) from a length of approximately 12 m, and from 10 m for the permanent ones (P-SLS).

For the case of *DRF*, the performance of the solution increases significantly, since, for the same lengths, total values of 0.63 to 0.97 and permanent values of 0.55 and 0.97 are obtained, showing that the inclusions are able to reduce almost completely the differential displacements. Even inclusions of only 5 m in length allow reducing the maximum differential displacement by 30%.

For the tunnel, inclusions of 5 m in length would be enough to meet the limit states, both for total settlements and angular distortion. For the perimeter beam, the piles are sufficient for the limit states not to be exceeded.

The performance of the inclusions for settlement control of the tunnel and the perimeter beam, compared to that of the raft, is lower, since these elements are already reinforced with piles, i.e., the inclusions work together with the piles to reduce the settlements. Figure 10 shows the axial load developed in a central pile of the perimeter beam and tunnel, and in a central rigid inclusion, for the analyzed cases. It is possible to observe that when the inclusions are added, the load on the piles substantially decreases, mainly in the tunnel zone (Figure 10b), where the maximum load goes from 1162 kN to 833 kN, i.e., a reduction of approximately 30%. This reduction is due to the stiffness increase caused by the presence of rigid inclusions, which absorbs a significant portion of the external load when the silo is filled (Figure 10c).

The good performance observed in reducing the raft settlements is also reflected in the behavior of the raft-perimeter beam structural joint (gap opening), as shown in Figure 11. For the case of the original foundation, a gap opening of up
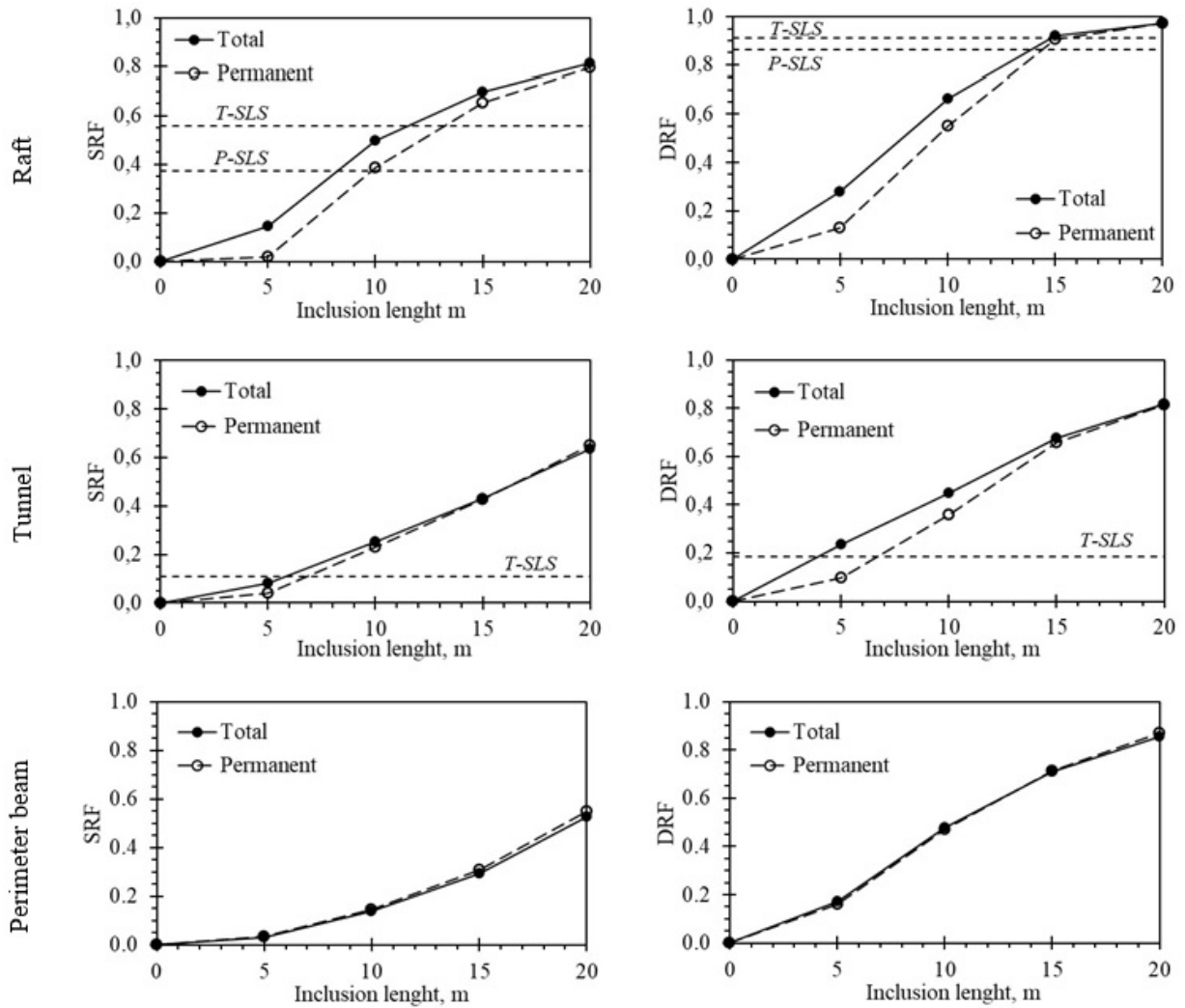
Figure 9. *SRF* and *DRF* factors obtained for different inclusion lengths, at the raft, tunnel, and perimeter beam for total and permanent displacements.
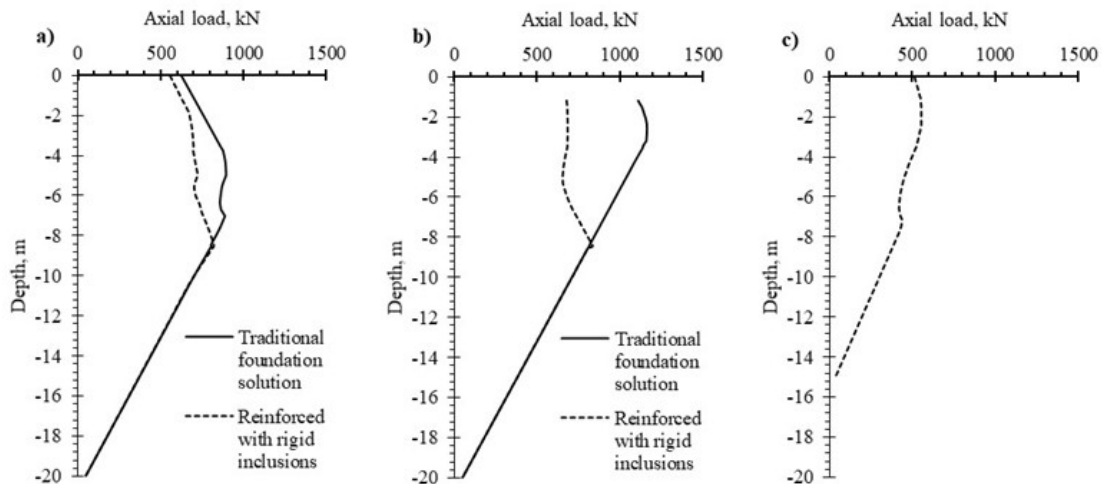

Figure 10. Axial load developed at: (a) perimeter beam piles; (b) tunnel piles; (c) inclusions.

to 15.2 cm was calculated. When the inclusions are placed, this value drops considerably to 5.7 cm ($GRF = 0.62$) and 1.3 cm ($GRF = 0.91$), for 10 and 20 m lengths, respectively.

5.2 Case 2: group behavior

According to the combinations defined in Figure 5, the vertical displacements obtained for the three load combinations, considering the natural moisture state and the original foundation are shown in Figure 12. In general, for the filled silos, vertical displacements increase mainly in the direction of the axes of symmetry X, and for the empty ones in the direction of the filled silo.

When compared to the values obtained for the individual silo, the maximum vertical displacement (ρ^{MAX}) for combination 1 (Figure 12a) increases by 5% (from 34 to 35.6 cm) for the external silos (filled), and for the internal ones (empty) $\rho^{MAX} = 4.1$ cm. For combination 2 (Figure 12b) ρ^{MAX} increases by 8% (up to 36.6 cm) for the internal ones, and again $\rho^{MAX} = 4.1$ cm for the empty ones. Finally, for combination 3 (Figure 12c, all silos filled), ρ^{MAX} increases by 11% (up to 37.8 cm) for the internal ones, and by 8% for the external.

When rigid inclusions are considered, the vertical displacement increase follows the same tendency verified for the original foundation. In the alternative solution compared to the individual silo analysis, ρ^{MAX} values increase more significantly for the filled silos, for combinations 1, 2, and 3, ρ^{MAX} increases by 15%, 23%, and 29% (from 10 to 11.5 cm, 12.3 cm, and 12.9 cm), respectively, but all of them below the established limit-state. For the empty silos $\rho^{MAX} = 3.3$ cm, for both cases (combinations 1 and 2).

Table 5 summarizes the values of the *SRF*, *DRF*, and *GRF* obtained for the performance evaluation of the group of silos for all the analyzed combinations. Although the values of ρ^{MAX} increased by up to 29% in relation to the analysis of an individual silo, the *SRF* values decreased by only 6% (from 0.70 to 0.66), while *DRF* and *GRF* remained practically the same. Small performance values were obtained for the empty silos, because the calculated total and differential vertical displacements, both with and without inclusions, were low, i.e., both cases were well below the established limit-state.

The results show that, for the analyzed case, the performance of the foundation reinforced with rigid inclusions is little affected by the operation of a group of silos.
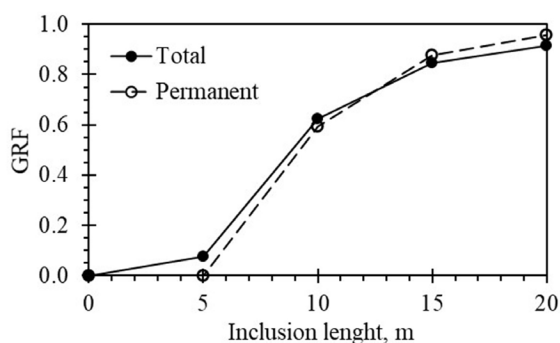

Figure 11. *GRF* factor obtained for total and permanent displacements.
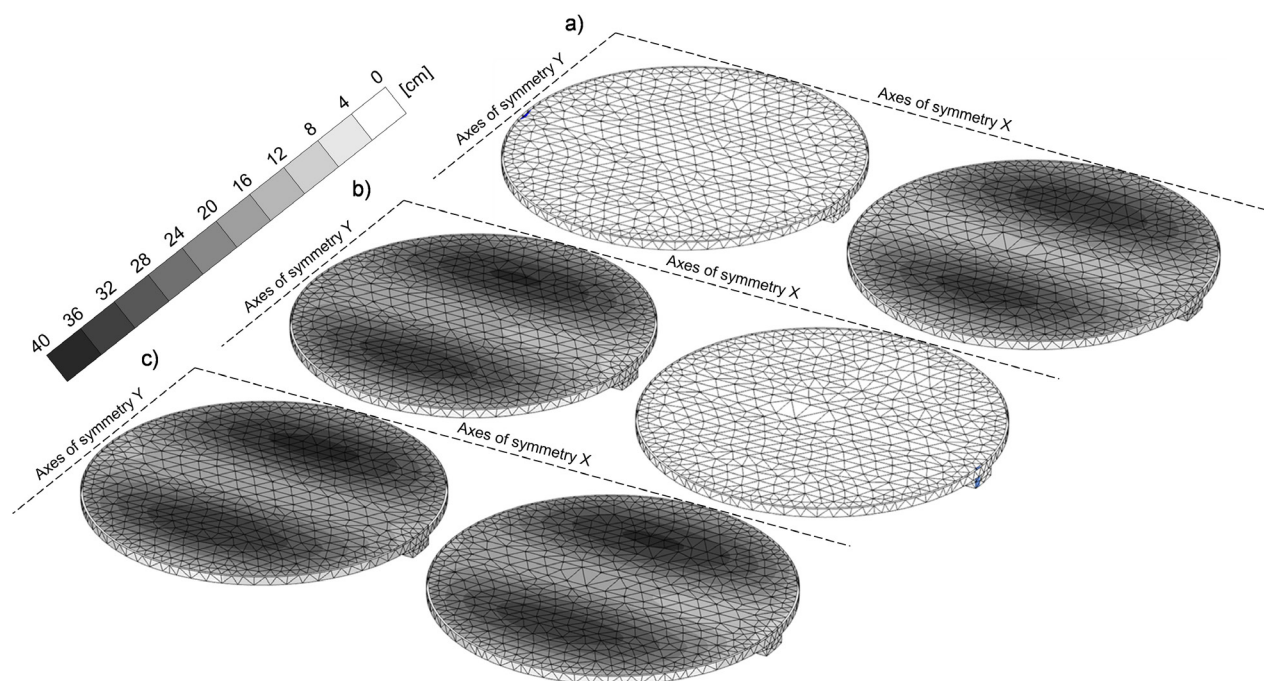

Figure 12. Vertical displacements computed for the silos group with the original foundation, when a) external silos are filled (combination 1), b) when internal silos are filled (combination 2) and c) when all silos are filled (combination 3).

Table 5. Performance evaluation of silos group for different filling combinations.

Comb.	Silos	*SRF*	*DRF*	*GRF*
	Individual silo behavior	0.70	0.92	0.84
1	External (01, 04, 05, 08)	0.67	0.90	0.83
	Internal (02, 03, 06, 07)	0.17	0.17	0.09
2	External (01, 04, 05, 08)	0.20	0.20	0.13
	Internal (02, 03, 06, 07)	0.66	0.90	0.84
3	External (01, 04, 05, 08)	0.66	0.92	0.84
	Internal (02, 03, 06, 07)	0.66	0.93	0.85

6. Conclusions

This article presents the evaluation of the performance of grain silos reinforced by rigid inclusions in soils characteristic of the Central-West region of Brazil, during its construction and operation, through three-dimensional numerical modeling. The main conclusions are summarized below:

a) SLS values of 150 mm and 1/400, for vertical settlement and angular distortion, respectively, are suggested for the foundation design of grain silos.

b) For the original foundation solution, the calculated displacement values considerably exceed the adopted limit state for total vertical displacements. When rigid inclusions were added, it was possible to observe that, from 10 m in length, a good performance of the foundation system was obtained. The inclusions were able to reduce the maximum total and differential displacements by around 80%. Even inclusions of only 5 m in length allow to reduce the maximum differential displacement by 30%.

c) It was shown that the maximum performance obtained with the inclusions was in the control of the differential displacements for all the structural elements of the foundation, thus, reducing the probability of structural failures.

d) The presence of rigid inclusions causes a reduction (of approximately 30%) in the load absorbed by the tunnel piles, due to the stiffness increase beneath the raft. Hence, the quantity of piles could be optimized, or even totally replaced by rigid inclusions.

e) The good performance observed in reducing the raft settlements was also reflected on the behavior of the structural joint (gap opening), obtaining a reduction of the gap opening up to 91%. It is possible to say that one way to further reduce this value would be to reduce the length or number of the piles beneath the perimeter beam, which will lead to an optimized design.

f) For the analyzed case, the performance of the foundation reinforced with inclusions is little affected when considering the silos working as a group. Thus, the execution of the parametric analysis for the foundation design, i.e., to determine the length, diameter, and the number of inclusions and/or piles, can be done using an isolated silo. However, for the final review of the SLS, the foundations should be analyzed considering the silos working as a group.

The rigid inclusion system proved to be an efficient foundation solution that allows controlling total and differential settlements during the serviceability stage of the silo, helping to prevent the formation of cracks in the structural elements and grain contamination by the excessive opening of the raft-perimeter beam joint.

Acknowledgements

Declaration of interest

The authors have no conflicts of interest to declare. All co-authors have observed and affirmed the contents of the paper and there is no financial interest to report.

Authors' contributions

Juan Félix Rodríguez Rebolledo: conceptualization, formal analysis, funding acquisition, investigation, methodology, project administration, resources, software,

supervision, validation, visualization, writing – original draft. Isabelle Moreira Santiago: conceptualization, formal analysis, investigation, methodology, software, validation, visualization, writing – original draft. Heitor Cardoso Bernardes: conceptualization, investigation, methodology, validation, visualization, writing – review & editing. Thiago Augusto Mendes: investigation, methodology, visualization, writing – review & editing.

List of symbols

A	Cross section area
a	Diameter of the inclusion cap
c'	Effective soil cohesion
D	Diameter
d	Plate thickness
DRF	Angular distortion reduction factor
E	Young's modulus
E_{50}^{ref}	Reference secant stiffness modulus for the drained triaxial test
E_{oed}^{ref}	Reference tangent stiffness modulus for oedometric loading
E_{ur}^{ref}	Reference stiffness modulus for unloading and reloading conditions
F_{max}	Pile base resistance
g_c	Inclination factor of the load transfer cone
G^{MAX}	Maximum gap between the perimeter beam and the raft
GRF	Gap opening reduction factor
H	Distribution layer thickness
K_o^{nc}	Coefficient of the earth pressure at rest for normal consolidation
K_0	Coefficient of earth pressure at rest
L	Distance / length
m	Exponent that defines the stress-strain dependence
N_c, N_q	Bearing capacity factors
POP	Pre-overburden pressure
q_1	Total pressure transmitted to the inclusion cap
q_s	Uniformly distributed load over the raft
q_{ult}	Ultimate load-bearing capacity of the inclusion cap
p^{REF}	Reference isotropic stress
R_f	Failure ratio
S	Spacing between inclusions
s_c	Shape factor
SRF	Settlement reduction factor
T_{sf}	Pile side friction resistance
β	External angle of the load transfer cone
γ	Soil unit weight
Δ	Variation / difference of a variable with respect to two points
δ	Angular distortion
ν	Poisson's ratio
ν_{ur}	Unloading/reloading Poisson's ratio
ρ	Vertical displacement / settlement
ϕ'	Effective shear angle
ψ	Dilatancy angle

References

ABNT NBR 6118. (2014). *Design of Structural Concrete - Procedure*. ABNT - Associação Brasileira de Normas Técnicas, Rio de Janeiro, RJ (in Portuguese).

ABNT NBR 6122. (2019). *Design and Construction of Foundations*. ABNT - Associação Brasileira de Normas Técnicas, Rio de Janeiro, RJ (in Portuguese).

ABNT NBR 6484. (2001). *Soil - Standard Penetration Test - SPT - Soil Sampling and Classification - Test Method*. ABNT - Associação Brasileira de Normas Técnicas, Rio de Janeiro, RJ (in Portuguese).

ABNT NBR 7821. (1983). *Tanques soldados para armazenamento de petróleo e derivados - Anexo C: Fundações*. ABNT - Associação Brasileira de Normas Técnicas, Rio de Janeiro, RJ (in Portuguese).

ASIRI National Project. (2011). *Recommendations for design, construction and control of rigid inclusion ground improvements*. Presses des Ponts.

Bahar, R., Sadaoui, O., & Amzal, D. (2013). Differential settlements of cylindrical steel storage tanks: case of the marine terminal of Bejaia. In *Proceedings International Conference on Case Histories in Geotechnical Engineering*, Chicago. Retrieved in May 5, 2021, from https://scholarsmine.mst.edu/icchge/7icchge/session02/12.

Becker, D.E., & Lo, K.Y. (1979). Settlement and load transfer of ring foundation for tower silos. *Canadian Agricultural Engineering*, 21(2), 97-110. Retrieved in May 5, 2021, from https://library.csbe-scgab.ca/docs/journal/21/21_2_97_ocr.pdf

Bernardes, H.C., Souza Filho, H.L., Dias, A.D., & Cunha, R.P. (2021). Numerical analysis of piled raft foundations designed for settlement control on steel grain silo in collapsible soils. *International Journal of Civil Engineering*, 19, 607-622. http://dx.doi.org/10.1007/s40999-020-00586-5.

Bernuy, C., Hor, B., Kim, S., Song, M., & Alqoud, S.Y. (2018). LNG tanks on rigid inclusions: kuwait. *Innovative Infrastructure Solutions*, 3(80), 1-12. http://dx.doi.org/10.1007/s41062-018-0186-8.

Briançon, L., Dias, D., & Simon, C. (2015). Monitoring and numerical investigation of a rigid inclusions-reinforced industrial building. *Canadian Geotechnical Journal*, 52(10), 1592-1604. http://dx.doi.org/10.1139/cgj-2014-0262.

Cardoso, F.B.F. (2002). *Properties and mechanical behavior of soils of the Brazilian Central Plateau* [Doctoral thesis, University of Brasilia]. University of Brasília's repository (in Portuguese). https://repositorio.unb.br/handle/10482/31224.

Coelho, R.S. (2013). *Relatório das sondagens executadas na área destinada à construção da obra casa do professor*. FUNDEX. Brasília. (in Portuguese).

Combarieu, O. (1990). Amelioration of soils by vertical rigid piles, for shallow foundation. *Revue Française de Géotechnique*, 53, 33-44. http://dx.doi.org/10.1051/geotech/1990053033. (in French).

Companhia Nacional de Abastecimento – CONAB. (2022). *Boletim da Safra de Grãos - 5° Levantamento. Safra 2021/22: Tabela de dados - Produção e balanço de oferta e demanda de grãos*. CONAB (in Portuguese). Retrieved in March 5, 2022, from https://www.conab.gov.br/info-agro/safras/graos/boletim-da-safra-de-graos

Conciani, W. (2016). *Possíveis melhoramentos no projeto e construção de silos* [Candidature Thesis for Full Professor]. Instituto Federal de Educação, Ciência e Tecnologia de Brasília. (in Portuguese).

Cruz, P.T. (1987). Solos residuais: algumas hipóteses de formulações teóricas de comportamento. In *Seminário em Geotecnia de Solos Tropicais* (pp. 79-111). ABMS-UnB. (in Portuguese).

D'Orazio, T.B., & Duncan, J.M. (1987). Differential settlements in steel tanks. *Journal of Geotechnical Engineering*, 113(9), 967-983. http://dx.doi.org/10.1061/(ASCE)0733-9410(1987)113:9(967).

Dogangun, A., Karaca, Z., Durmus, A., & Sezen, H. (2009). Cause of damage and failures in silo structures. *Journal of Performance of Constructed Facilities*, 23(2), 65-71. http://dx.doi.org/10.1061/(ASCE)0887-3828(2009)23:2(65).

Echevarría, S.P. (2006). *Soil arching effects due to earth fills supported by piles foundations* [Master's dissertation, University of Brasilia]. University of Brasília's repository (in Portuguese). https://repositorio.unb.br/handle/10482/3776.

García-Buriticá, J.A. (2021). *Study of the load-transfer mechanism in the distribution layer of foundations reinforced by rigid inclusions* [Doctoral thesis, University of Brasilia]. University of Brasília's repository (in Portuguese). https://repositorio.unb.br/handle/10482/41295.

García-Buriticá, J.A.B., Rodríguez-Rebolledo, J.F., Mutzenberg, D.V., Caicedo, B., & Gitirana Junior, G.F.N. (2021). Experimental investigation of a load-transfer material for foundations reinforced by rigid inclusions. *Journal of Geotechnical and Geoenvironmental Engineering*, 147(10), 04021110. http://dx.doi.org/10.1061/(ASCE)GT.1943-5606.0002649.

Guimarães, R.C. (2002). *Analysis of properties and behavior of a lateritic soil profile applied to the study of the bearing capacity of bored piles* [Master's dissertation]. University of Brasília (in Portuguese).

IS 1904. (1986). *Code of practice for design and construction of foundations in soils: general requirements*. Indian Standard, New Delhi.

Jardim, N.A. (1998). *Metodologia de previsão de capacidade de carga vertical e horizontal com o dilatômetro de Marchetti* [Master's dissertation]. University of Brasília. (in Portuguese).

Móczár, B., Mahler, A., Lódör, K., & Bán, Z. (2016). Back analysis of settlements beneath the foundation of a sugar silo by 3D finite element method. *Plaxis Bulletin*, 39, 12-17.

Mota, N.M.B. (2003). *Ensaios avançados de campo na argila porosa não saturada de Brasília: interpretação e aplicação em projetos de fundação* [Doctoral thesis]. University of Brasília (in Portuguese).

Otálvaro, I.F. (2013). *Comportamento hidromecânico de um solo tropical compactado* [Doctoral thesis, University of Brasilia]. University of Brasília's repository (in Portuguese). https://repositorio.unb.br/handle/10482/13591.

Pecker, A. (2004). Design and construction of the rion antirion bridge. In *Proceedings Geotechnical Engineering for Transportation Projects*, Los Angeles, California. (Vol. 1, pp. 216-240). Reston: ASCE. https://doi.org/10.1061/40744(154)7.

Perez, E.N.P. (1997). *O uso da teoria da elasticidade na determinação do módulo de Young de solo adjacente a estacas carregadas verticalmente na argila porosa de Brasília* [Master's dissertation]. University of Brasília (in Portuguese).

Pérez-León, R.F. (2017). *Rigid Inclusions for controlling settlement in collapsible soils of the Federal District* [Master's dissertation, University of Brasilia]. University of Brasília's repository (in Portuguese). https://repositorio.unb.br/handle/10482/24065.

Rodríguez-Rebolledo, J.F., & Auvinet, G. (2006). Rigid inclusions in Mexico City soft soils. In *International Symposium Rigid Inclusions in Difficult Soft Soil Conditions* (ISSMGE TC-36, Vol. 1, pp. 197-206), Mexico City.

Rodríguez-Rebolledo, J.F., Pérez-León, R.F., & Camapum De Carvalho, J. (2019a). Obtaining the mechanical parameters for the hardening soil model of Tropical soils in the city of Brasília. *Soils and Rocks*, 42(1), 61-74. http://dx.doi.org/10.28927/SR.421061.

Rodríguez-Rebolledo, J.F., Pérez-León, R.F., & Camapum de Carvalho, J. (2019b). Performance evaluation of rigid inclusion foundations in the reduction of settlements. *Soils and Rocks*, 42(3), 265-279. http://dx.doi.org/10.28927/SR.423265.

Sales, M.M. (2000). *Análise do comportamento de sapatas estaqueadas* [Doctoral thesis]. University of Brasília (in Portuguese).

Sales, M.M., Vilar, O.M., Mascarenha, M.M.A., Silva, C.M., Pereira, J.H.F., & Camapum de Carvalho, J. (2015). Fundações em solos não saturados. In J.C. Carvalho, G.F.N. Gitirana Junior, S.L. Machado, M.MA. Mascarenha & F.C. Silva Filho (Eds.), *Solos não saturados no contexto geotécnico* (pp. 651-685). ABMS. (in Portuguese).

Santoyo, E., & Ovando, E. (2006). Geotechnical considerations for hardening the subsoil in Mexico City's Metropolitan Cathedral. In *International Symposium Rigid Inclusions in Difficult Soft Soil Conditions* (ISSMGE TC-36, Vol. 1, pp. 171-178), Mexico City.

Santrač, P., Bajić, Ž., Grković, S., Kukaras, D., & Hegediš, I. (2015). Analysis of calculated and observed settlements of the silo on loess. *Hrčak Technical Gazette*, 22(2), 539-545. http://dx.doi.org/10.17559/TV-20140615132437.

Souza Filho, H.L. (2018). *Estudo da técnica de sistemas em radier estaqueado para fundações de silos graneleiros do Centro-Oeste* [Master's dissertation, University of Brasilia]. University of Brasília's repository (in Portuguese). https://repositorio.unb.br/handle/10482/34449